•水利与土木工程•

DOI:10.12454/j.jsuese.202500984

本刊网刊

融合时序InSAR技术的灌区滑坡易发性评价

王陈浩[1,2],周　俊[3],邓　斌[1,2*],何沛庭[1],欧阳君[4],余文杰[1,4],蒋昌波[1,2]

(1.长沙理工大学 水利与海洋工程学院,湖南 长沙 410114;2.洞庭湖水环境治理与生态修复湖南省重点实验室,湖南 长沙 410114;
3.湖南省水利发展投资有限公司,湖南 长沙 410007;4.湖南省水利水电勘测设计规划研究总院有限公司,湖南 长沙 410007)

摘　要:山区水利工程地质条件复杂,滑坡灾害频发,严重威胁区域安全和可持续发展。本文以犬木塘灌区为例,构建一种融合InSAR(interferometric synthetic aperture radar)技术的滑坡易发性评价模型,从地形地貌、地质条件、自然环境和人类活动4个方面选取14个静态评价因子,并基于SBAS–InSAR(small baseline subset–InSAR)技术提取地表形变速率作为动态因子。采用信息量法对评价因子进行无量纲处理,分别构建随机森林(RF)、支持向量机(SVM)和卷积神经网络(CNN)3类模型,并通过曲线下面积(AUC)、准确率、精准率、召回率和F1分数对模型性能进行综合评估。结果表明:3类模型的易发性分区在空间分布上具有较高一致性,其中,SVM模型综合表现最优,其次为CNN模型,RF模型相对较弱;引入InSAR形变因子后,RF–InSAR与CNN–InSAR模型的部分性能指标有所提升,SVM–InSAR模型各项性能指标得到显著改善,其中,AUC值较RF–InSAR和CNN–InSAR模型分别提升4.2%和0.4%。融合时序InSAR技术的滑坡易发性评价方法可显著提升模型精度,为山区水利工程建管、工程滑坡防治及灾害管理提供技术支持。

关键词:滑坡易发性评价;SBAS–InSAR;机器学习模型;卷积神经网络;犬木塘灌区工程

中图分类号:TV67;TP75　　**文献标志码:**A　　**文章编号:**2096-3246(2026)06-0268-14

大型水利工程(如水库、灌区)在优化水资源配置等方面发挥着重要作用。然而在实际运营过程中,工程面临着自然环境、人类活动及结构变形等多重风险。受全球气候变化影响,地质灾害发生频率显著增加[1–2],其中滑坡是灌区常见、极具威胁性的灾害之一,主要由气象、水文、风化等自然因素与人类活动共同诱发,表现为斜坡岩土体的渐进变形与失稳破坏。山区水利工程多处于地质条件复杂的地区,在极端降雨作用下极易被诱发山体滑坡,严重威胁工程与设施安全[3–6]。因此,针对山区水利工程开展滑坡形变监测及易发性评价研究十分必要[7–9]。

随着"3S"技术的高速发展,大量对地观测卫星升空,遥感技术在滑坡灾害监测方面得到了广泛应用。其中,合成孔径雷达干涉测量技术(InSAR)凭借全天候、高精度和广范围监测优势,为滑坡监测和早期识别提供有效的技术支撑[10–12]。以斯坦福永久散射体[13](StaMPS)和小基线集[14](SBAS)为代表的时序InSAR技术,已被广泛应用于滑坡诱发机理及灾害早期识别研究。例如:张永双等[15]利用InSAR技术判别高山峡谷古滑坡复活的阶段,将初始拉裂变形向匀速变形的拐点视为复活起点标志;董玉娟等[16]联合DS–InSAR技术和空间聚类方法,在澜沧江流域识别出6处显著变形滑坡体。此外,万鹏[17]、Wang[18]、Bian[19]和Zhu[20]等亦开展了类似的研究。在获取形变信息的基础上,滑坡易发性评价已成为研究热点,其基于"历史滑坡在相似条件下可能再次发生"假设,主要有定性方法[21–23]、定量方法[24–26]及两者耦合的方法,如潘网生[27]、李成林[28]、张妤涵[29]和Zhang[30]等利用机器学习或深度学习模型预测未来滑坡空间分布。然而,现有研究中所选评价因子多集中于地质、水文等静态因

收稿日期:2025 – 12 – 23　　**修回日期:**2026 – 03 – 09　　**网络出版日期:**2026 – 03 – 09

基金项目:国家自然科学基金面上项目(51979015);湖南省科技创新计划项目(2020RC3037;20hnkj019);湖南省水利科技项目(XSKJ2025056–33);犬木塘水库工程科技创新项目(2023430102004600)

作者简介:王陈浩(1993—),男,博士生. 研究方向:水动力学与水利信息化. E-mail:Francis_Wang.Chenhao@outlook.com

* **通信作者:**邓　斌,教授, E-mail:dengbin07@csust.edu.cn

子，对地表形变等动态因子的关注相对不足。InSAR 技术能够提取地表形变速率反映滑坡演变状态，将其作为动态因子融入滑坡易发性评价模型，有助于弥补传统模型动态响应能力的不足，从而提高滑坡易发性评价的准确性和时效性[31]。

犬木塘水库工程为湖南目前在建规模最大的水利工程，其灌区工程位于湖南省中部山区，地质条件复杂，对工程建设和区域发展构成严重威胁。在多部门协同管理背景下，开展精细化、动态化的滑坡监测与易发性分区具有现实意义。本文以犬木塘灌区为研究对象，开展山区水利工程滑坡易发性评价，探讨将时序 InSAR 技术融入传统评价模型的优化效果，并对研究区进行滑坡易发性分区。研究成果可为灌区工程滑坡监测预警与风险防控提供科学依据与技术支撑。

1　研究区概况及研究方法

1.1　研究区概况

犬木塘灌区位于湖南省中部。研究区处于丘陵与山地过渡带，地势总体呈西南高、东北低分布，海拔范围为 56～1 498 m，地形起伏较大，具备滑坡发育的基本地貌条件，在复杂地质构造及工程扰动背景下，滑坡灾害发育显著。

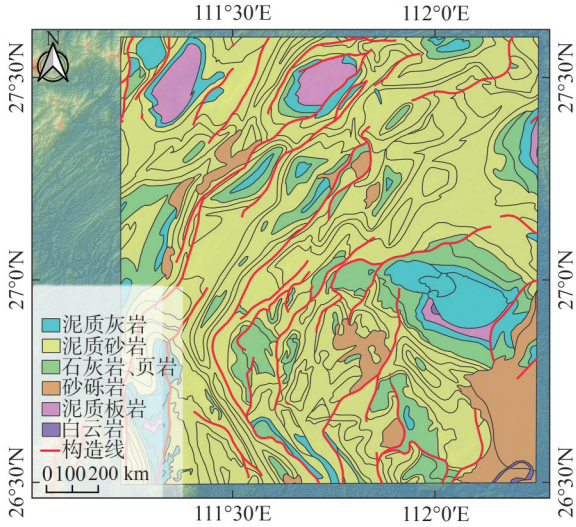


图 1　研究区地理信息概况

Fig. 1　Study area geographic information overview

1）区域构造背景控制。研究区位于新华夏系与祁阳山字形弧形构造前弧外带的复合部位，构造活动明显，断层与褶皱构造发育。长期构造应力作用使岩体节理裂隙密集发育，形成多组结构面及潜在滑移面，为滑坡形成提供了结构条件。构造破碎带内岩体完整性差，抗剪强度降低，在降雨及工程扰动作用下易发生失稳。

2）岩性组合与软弱层控制。研究区出露地层自奥陶系（O）至第四系（Q）较为完整。区内岩性以灰岩等碳酸盐岩及砂砾岩等碎屑岩为主，广泛分布砂质板岩、泥质板岩等软弱岩层，在降雨入渗作用下遇水易软化，形成顺层滑动面，是控制研究区滑坡空间分布的重要内在因素。

3）水文气候条件作用。研究区强降雨或持续降雨过程增强坡体入渗，导致孔隙水压力升高、有效应力降低。地下水位波动及岩体软化进一步削弱坡体稳定性。在软弱岩层或构造破碎带内，水力作用与重力效应叠加，易诱发浅层滑坡或顺层滑动。

4）工程扰动与内外动力耦合。灌区内众多明渠、渡槽及边坡开挖工程沿山体布设。工程切坡打破了原有应力平衡削弱坡脚支撑条件，在构造破碎岩体、水文条件变化及工程扰动的共同作用下，形成多因素耦合型滑坡孕灾机制。

1.2　研究方法

本文的技术流程如图 2 所示。首先，利用 SBAS–InSAR 技术反演研究区广域地表形变速率，识别潜在滑坡风险隐患并分析其形变特征；基于地形地貌、地质条件、自然环境和人类活动 4 类影响因素收集多源评价因子，利用皮尔逊相关系数进行因子相关性检验，筛选出最终静态评价因子，与形变速率动态评价因子共同构建滑坡易发性评价因子；基于信息量模型提取各评价因子的信息量值，分别耦合随机森林模型、支持向量机模型和卷积神经网络模型构建滑坡易发性评价模型，通过网格搜索方法优化模型参数；最后生成滑坡易发性评价图，并利用准确率（Accuracy，记为 A）、精准率（Precision，记为 P）、召回率（Recall，记为 R）、F1 分数（F1–score，记为 F）等关键指标对模型结果进行对比分析。

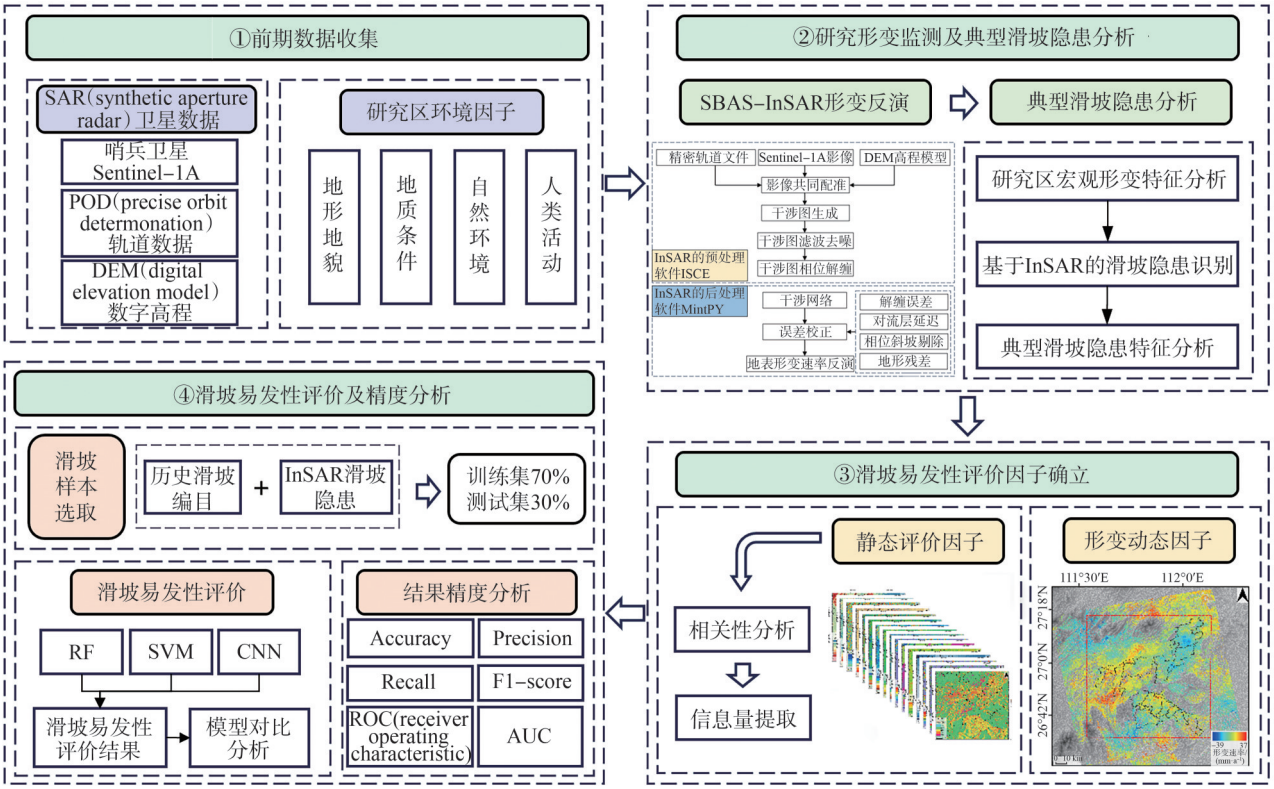


图2 研究技术流程图

Fig. 2 Research flowchart

1.2.1 信息量法

信息量法[32](IM)以信息论为基础,利用历史滑坡的密度特征计算不同评价因子分级区间下滑坡发生的信息量,以评估滑坡发生概率,计算式为:

$$I_i=\ln\frac{N_i/N}{S_i/S} \tag{1}$$

式中:I_i为评价因子i的信息量值,值越大滑坡越易发生;N_i为评价因子i各级的滑坡点数量;N为研究区总滑坡点个数;S_i为对应分级栅格面积;S为研究区总栅格面积。

1.2.2 随机森林

随机森林[33](RF)是一种基于决策树的集成学习算法。通过构建多个决策树并综合其预测结果提升分类性能。采用自助抽样方式从原始样本中随机抽取子样本构建决策树,并通过"投票"方式确定最终分类结果。

1.2.3 支持向量机

支持向量机(SVM)[34]利用核函数将样本映射至高维特征空间,在滑坡和非滑坡之间构建最大间距超平面,实现最优分类。假设样本评价因子组成空间向量$\boldsymbol{X}_j=[x_1,x_2,x_3,\cdots,x_i]$($j$为空间向量顺序),对应训练样本为$(X_j,y_j)$,其中,$y_j$为第$j$个空间向量的分类标签,则决策函数$f(x)$为:

$$f(x)=\boldsymbol{w}\Phi(x)+b \tag{2}$$

式中,$\boldsymbol{w}$为超平面的法向量,$\Phi(x)$为核函数(本文采用径向核函数),b为阈值。

1.2.4 卷积神经网络

卷积神经网络[35](CNN)是一种深度学习算法,具有局部连通性和权值共享的特点,由输入层、卷积层、池化层、全连接层和输出层构成,可自动提取数据空间特征进行分类。

1.2.5 精度评价

本文利用混淆矩阵中的准确率、精准率、召回率、F1分数、受试者工作特征曲线(receiver operating characteristic curve)和曲线下面积AUC(area under the curve)等指标综合评估模型性能。T_P和T_N为正确预测滑坡点和非滑坡点数量,F_P和F_N为错误预测滑坡点和非滑坡点数量。各指标计算方法如下:

$$\begin{cases} A=\dfrac{T_P+T_N}{T_P+T_N+F_P+F_N}, \\ P=\dfrac{T_P}{T_P+F_P}, \\ R=\dfrac{T_P}{T_P+F_N}, \\ F=\dfrac{2PR}{P+R} \end{cases} \tag{3}$$

1.3 数据来源

在确保数据客观和易获取的前提下,选取包括地形地貌(高程、坡度、坡向、曲率、平面曲率、剖面曲率、

地形起伏度、地表粗糙度、地形湿度指数，均可由高程因子提取）、地质构造（地质年代、距断层距离）、人类活动（距道路距离、土地利用）和自然环境（植被指数、降雨量、距水系距离），共 16 个静态评价因子（表 1）。研究采用 30 m×30 m 栅格作为最小评价单元，将研究区划分成 3 498×3 160 的规则网格。同时，收集了研究区历史滑坡编目共 318 个，用于模型训练。

表 1　数据来源

Tab. 1　Data sources

名称	数据来源	时间	分辨率
高程	地理空间数据云	2011 年	30 m
地质年代	中国数字地质图空间数据库	2001 年	1∶2 500 000
构造线（距断层距离）		2001 年	1∶2 500 000
道路（距道路距离）	Open Street Map	2015 年	1∶100 000
水系（距水系距离）	Open Street Map	2015 年	1∶100 000
降雨量	全球卫星降水计划	2019—2024 年	0.1°×0.1°
植被指数	地理空间数据云	2021 年 2 月	30 m
土地利用	全球土地利用数据库	2023 年	30 m

2　形变监测及滑坡易发性评价

2.1　静态因子共线性分析

为避免评价因子之间存在潜在共线性问题[36]，本文采用皮尔逊相关系数对各因子间相关性进行定量分析。若两个因子的相关系数绝对值大于 0.5，认为二者存在较强相关性。皮尔逊相关系数热力图如图 3 所示，地形起伏度、地表粗糙度和坡度之间相关系数均大于 0.9。考虑因子的代表性与独立性，剔除地表粗糙度和地形起伏度，选取第 2.2 节中余下的 14 个评价因子作为易发性评价模型的输入变量。

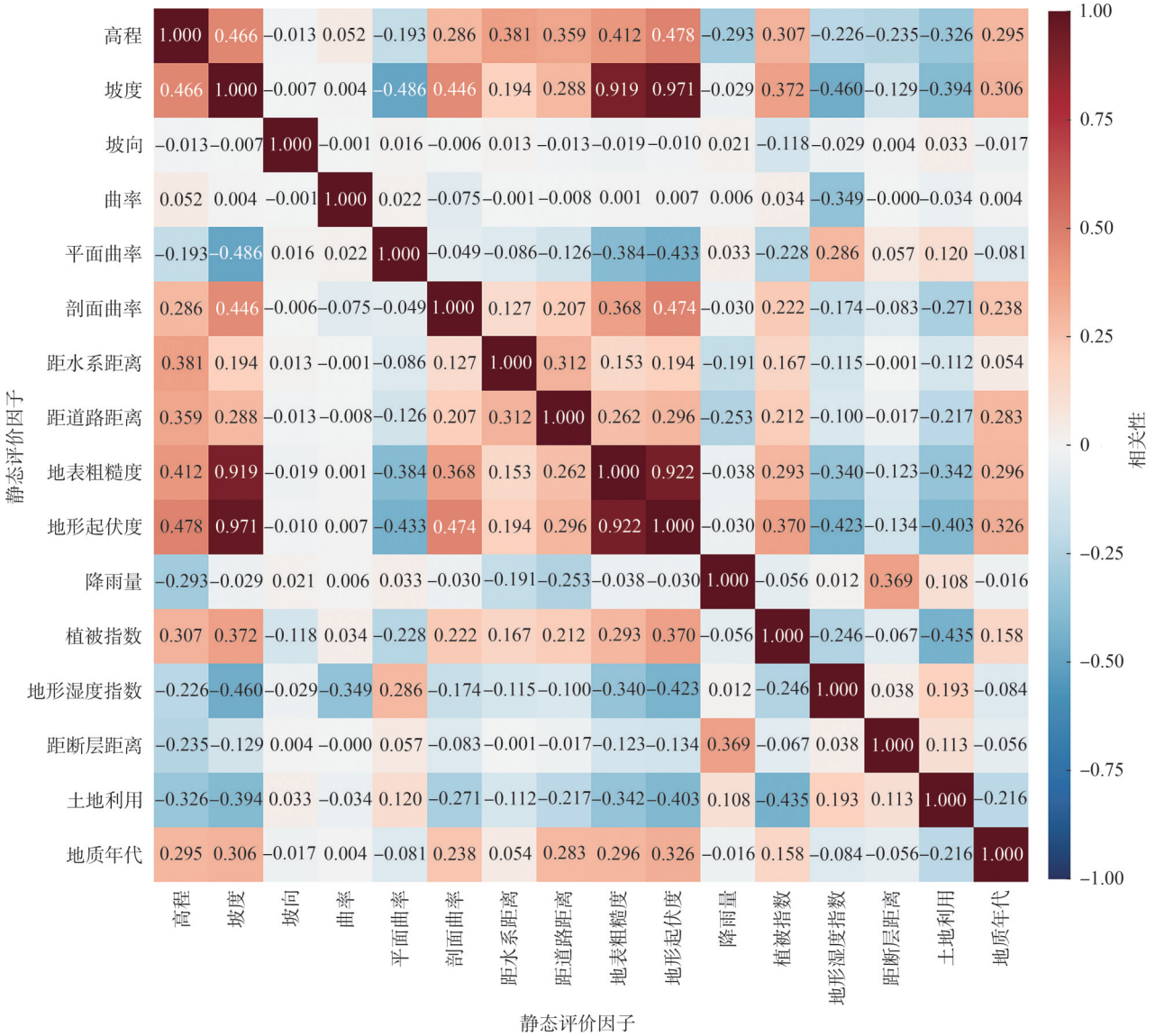


图 3　皮尔逊相关系数热力图

Fig. 3　Pearson correlation coefficients

2.2 因子分级

由于评价因子之间量纲差异较大，需对各因子进行无量纲处理。首先，依据经验法[37]或自然断点法[38]对评价因子进行初步分级，并基于信息量模型计算各分级区间的信息量值。相较于其他分级方法，信息量法具有计算简便、样本要求较低和可解释性强等特点。因此，本文利用信息量计算结果对分级区间进行优化调整，以减少类内方差并增强区分度，从而提升因子输入的区分能力。各静态评价因子分级后的空间分布如图4所示。图4中，NDVI为归一化植被指数。

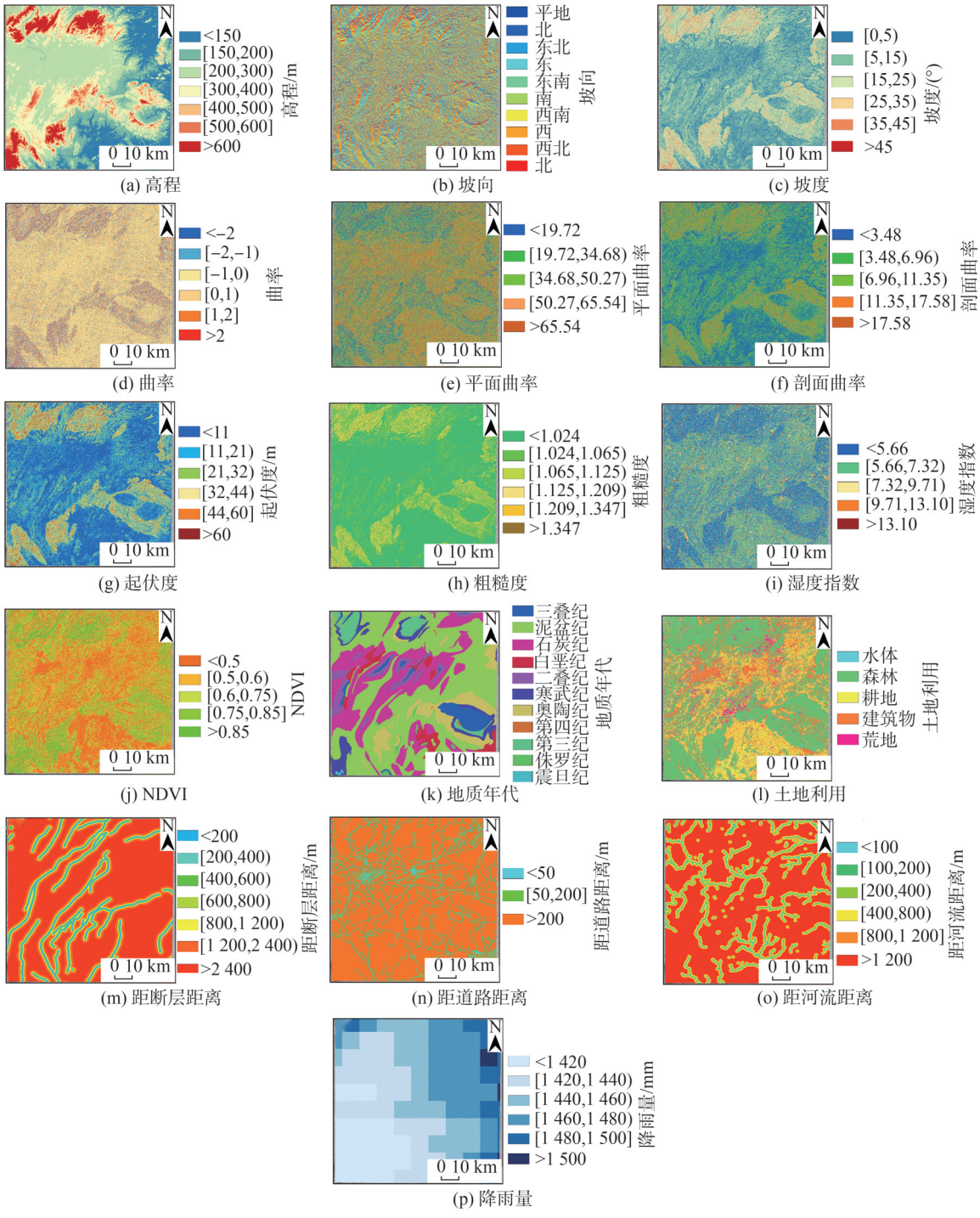


图4 静态评价因子空间分布

Fig. 4 Spatial distribution of static evaluation factors

2.3 动态评价因子

本文收集了覆盖研究区2020–07–18至2023–08–08的210景Sentinel–1A升轨SAR影像（Frame号81与86各80景），并同步获取对应精密定轨星历数据（POD）。首先，利用ISCE软件进行预处理，包括主从影像配准、生成干涉图、滤波和相位解缠等步骤，构建小基线集差分干涉

像对。然后，以时间基线阈值90 d、空间基线阈值500 m和平均相干性阈值0.3进行筛选，共获得321对干涉图像对。最后，利用SBAS–InSAR方法进行误差校正及时序处理，得到研究区地表形变速率。图5为研究区形变速率分布。

本文以±10 mm/a作为滑坡隐患识别的形变速率阈值，共识别出42处滑坡隐患区域，以Q1～Q42命名。其中，96%的隐患区域的中心速率超过−20 mm/a，其形变速率与空间形变特征如图6所示。

结合高分辨率光学影像与DEM地形特征分析，上述滑坡隐患区多表现为沿坡向展布的舌形或勺形形态，后缘存在弧形陡坎特征，前缘可见堆积鼓丘或坡脚隆起现象。根据岩性特征与坡体物质组成，研究区滑坡以板岩风化层及碎裂岩体控制的浅层岩质—碎屑质滑坡为主，局部第四系覆盖区表现为土质滑坡特征。为说明形变与

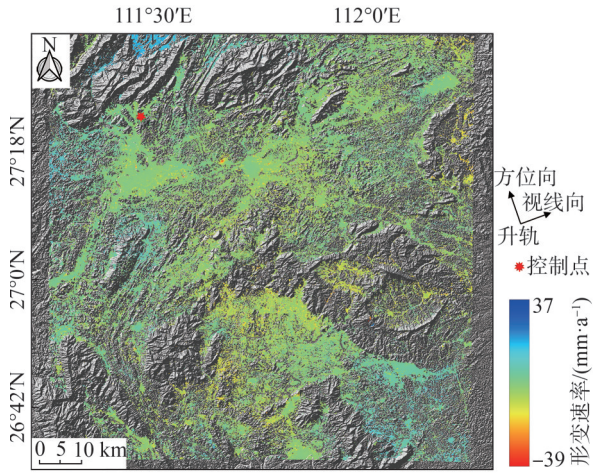
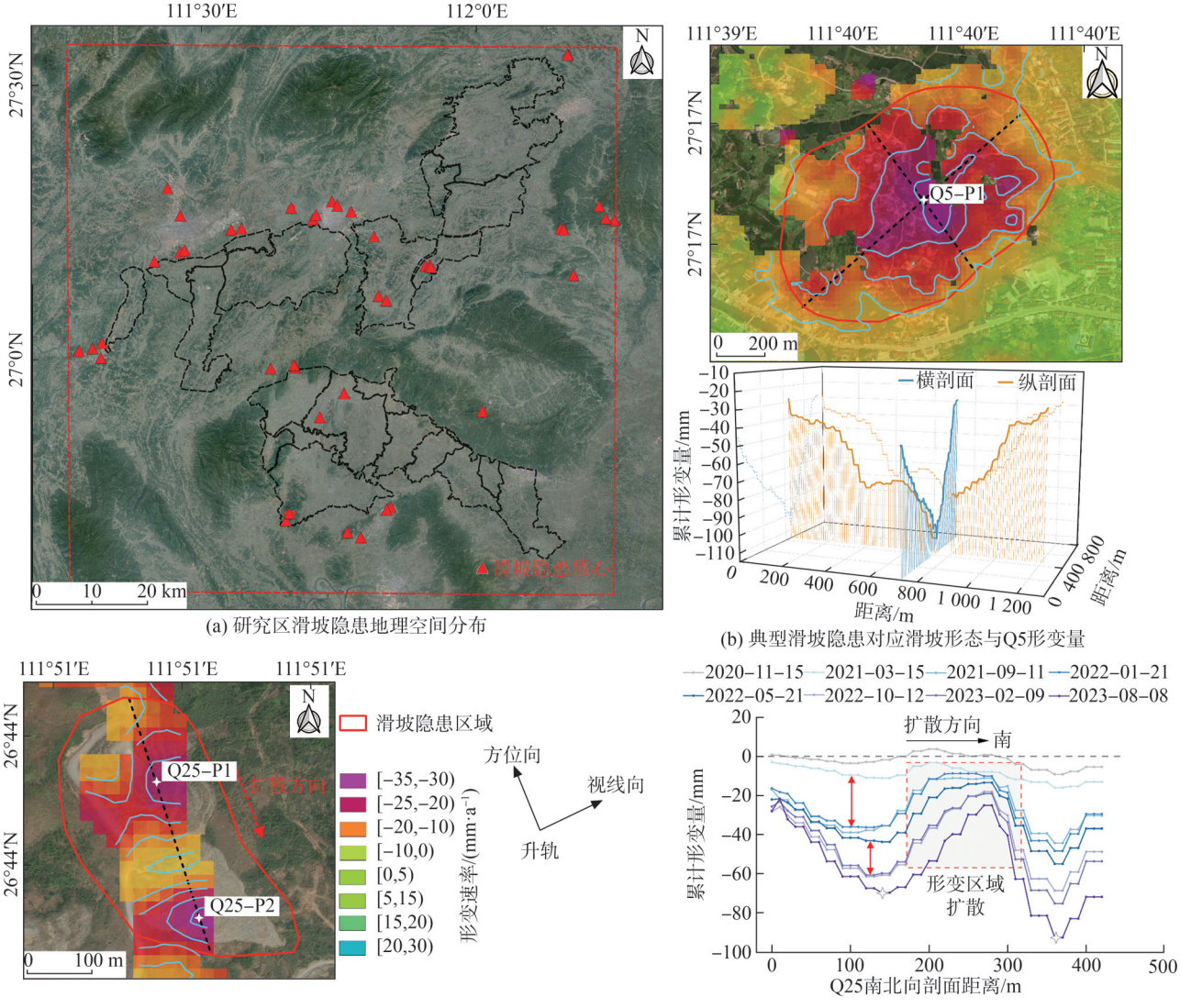


图5　研究区形变速率分布

Fig. 5　Time series InSAR deformation rate distribution in the study area



(a) 研究区滑坡隐患地理空间分布

(b) 典型滑坡隐患对应滑坡形态与Q5形变量

(c) 典型滑坡隐患对应滑坡形态与Q25形变量

图6　滑坡隐患地理空间分布和典型滑坡隐患的形变速率与空间形变特征

Fig. 6　Geographical spatial distribution of landslide hazards and the deformation rate and spatial deformation characteristics of typical landslide hazards

滑坡形态的对应关系，图6展示了Q5和Q25两个案例。Q5–P1位于沉降漏斗中心区域，靠近左侧坡体前缘，研究时段内累计形变量为−106.61 mm，表现出持续加速沉降的趋势，符合滑坡源区主滑动带的形变特征；针对Q25区域，Q25–P1与Q25–P2分别位于滑坡中上部滑体范围内，在2021–03–15至2021–09–11和2022–04–15至2022–10–12期间存在明显形变加速阶段（图6中红色箭头），最终形变量分别为−68.10 mm和−86.50 mm，伴随向南扩展的趋势，存在较高滑坡风险。综合形态特征、空间位置及形变演化规律分析，识别的滑坡隐患区域主要为活动性或潜在活动性滑坡，而非稳定古滑坡遗迹。

3 滑坡易发性结果分析

3.1 因子特征重要性

特征重要性反映评价因子在模型预测中的相对贡献，其数值越高，对模型输出结果影响越显著。本文通过训练后的机器学习模型进行分析获取了引入形变动态因子前后的特征重要性排序，如图7所示。结果表明，形变因子的特征重要性为0.066，处于中等水平，说明其在滑坡易发性判别方面具有一定贡献，可补充传统静态因子难以反映的时序特征，提高模型对潜在滑坡的识别能力。

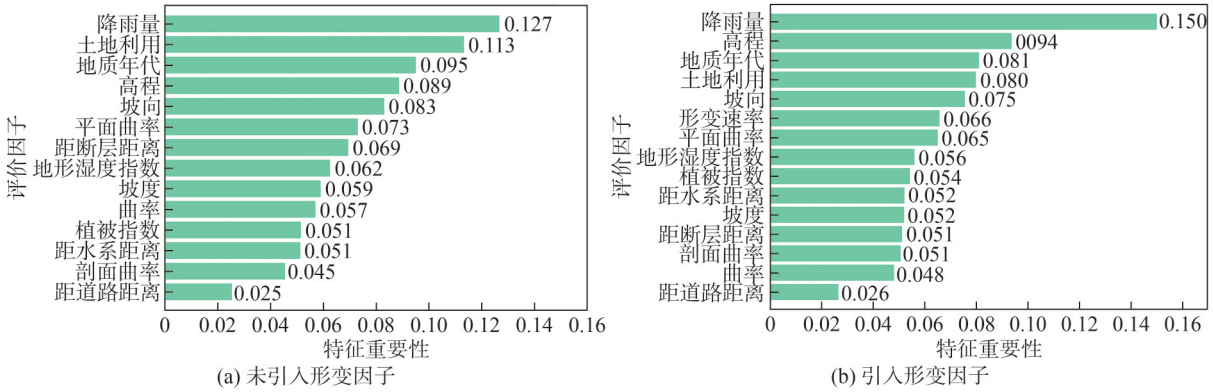


图7 引入形变因子前后评价因子特征重要性

Fig. 7 Comparison of feature importance of evaluation factors before and after introducing deformation factors

3.2 评价结果对比分析

本研究分别基于RF、SVM和CNN构建滑坡易发性评价模型。基于获取的滑坡样本数据，将2020年历史滑坡编目中的318处滑坡与InSAR识别出的42处滑坡隐患（共360处）标记为正样本，并建立1 000 m缓冲区[39–40]，叠加土地利用数据和Open Street Map建成区矢量数据，排除水域、城市建筑区内的异常点位，在缓冲区外随机生成等量360个非滑坡点作为负样本，以降低正样本数据混入负样本数据集的可能性并减弱空间自相关影响。最终将样本按70%与30%的比例划分为训练集（504个）和测试集（216个），分别用于训练和验证。

在此基础上，对引入形变速率动态因子前后的RF、SVM和CNN模型进行训练，得到研究区滑坡易发性栅格数据。在GIS环境中，利用自然断点法将结果划分为极低、低、中等、高和极高5个等级，如图7所示。同时提取各模型易发性分区的面积、滑坡密度及滑坡频率比等指标，评价模型性能，结果如表2所示。

由表2和图7可见，3类模型的易发性分区整体空间分布较为一致：高和极高易发区主要集中于研究区西部和北部山区，与近5 a平均降雨量分布具有较高一致性。该地区降雨量较大，通过入渗作用增加土壤含水量并增大孔隙水压力，从而降低岩土体有效应力与稳定性，促进了滑坡发育；而极低和低易发区主要分布于研究区西南部，该区域降雨量较小、地形相对平缓，且地质年代和土地利用存在差异，因此滑坡易发性较低。

在总体空间分布一致性的基础上，CNN模型与RF、SVM模型仍表现出一定差异，CNN模型的极低和低易发区面积占比较大，而极高易发区仍呈显著集中分布。该现象可能与CNN特征提取机制有关：相比依赖树型划分的RF模型和基于距离度量的SVM模型，CNN通过卷积运算提取空间邻域局部特征，对空间结构变化更为敏感，因此更倾向于将局部扰动较弱或形变特征不显著的区域划分为低易发区，从而导致低易发区面积提高。整体而言，引入形变动态因子前后，RF和SVM模型的评价结果较为接近，约40%的区域被划分为极低或低易发区；而CNN模型中两类低易发区面积占比超过了研究区的一半。尽管不同模型在分区面积上存在差异，但3类模型均显示大多数滑坡点集中于高和极高易发区，而低与极低易发区滑坡较少，与实际滑坡分布规律基本一致。进一步比较滑坡频率比可知，引入形变动态因子后，SVM–InSAR和CNN–InSAR模型在极低与极高易发区的滑坡频率比均得到不同程度提升，说明动态形变信息有助于提高模型对潜在不稳定区域的识别能力。从差异性上看，RF模型的滑坡频率比分区差异最为明显，SVM次之，CNN相对最弱，反映了CNN预测结果更为平滑、分区过渡更连续。总体

表 2　不同模型易发性指标对比

Tab. 2　Comparison of susceptibility indexes of different models

滑坡易发性等级分区	RF				SVM			
	面积/km^2	滑坡数/个	滑坡密度/(个·km^{-2})	滑坡频率比	面积/km^2	滑坡数/个	滑坡密度/(个·km^{-2})	滑坡频率比
极低易发区	1 822.93	2	0.001 1	0.03	2 838.75	13	0.004 6	0.13
低易发区	2 224.64	17	0.007 5	0.21	1 559.62	10	0.006 4	0.18
中等易发区	2 130.80	24	0.011 0	0.30	1 345.12	22	0.016 4	0.45
高易发区	2 064.10	57	0.027 7	0.76	1 517.19	56	0.036 9	1.02
极高易发区	1 705.84	260	0.158 9	4.39	2 650.20	259	0.097 7	2.69
滑坡易发性等级分区	CNN				RF–InSAR			
	面积/km^2	滑坡数/个	滑坡密度/(个·km^{-2})	滑坡频率比	面积/km^2	滑坡数/个	滑坡密度/(个·km^{-2})	滑坡频率比
极低易发区	4 764.16	26	0.005 5	0.15	1 802.36	5	0.002 7	0.08
低易发区	457.41	4	0.008 7	0.24	2 259.94	12	0.005 4	0.15
中等易发区	353.09	6	0.017 0	0.47	2 190.63	24	0.011 3	0.31
高易发区	432.58	7	0.016 2	0.45	2 059.42	48	0.023 3	0.64
极高易发区	3 941.07	317	0.080 4	2.22	1 635.96	268	0.157 1	4.34
滑坡易发性等级分区	SVM–InSAR				CNN–InSAR			
	面积/km^2	滑坡数/个	滑坡密度/(个·km^{-2})	滑坡频率比	面积/km^2	滑坡数/个	滑坡密度/(个·km^{-2})	滑坡频率比
极低易发区	2 789.51	6	0.002 2	0.06	5 345.83	33	0.006 2	0.17
低易发区	1 633.73	12	0.007 3	0.20	444.94	8	0.018 0	0.50
中等易发区	1 374.79	34	0.024 7	0.68	323.49	4	0.012 4	0.34
高易发区	1 510.41	51	0.033 8	0.93	395.10	10	0.025 3	0.70
极高易发区	2 602.43	257	0.098 8	2.72	3 438.92	305	0.088 7	2.45

而言，InSAR 形变因子的引入能够改善各模型在易发性等级区分方面的表现。

3.3　模型精度分析

图 8 展示了各模型滑坡易发性分区。图 9 展示了各模型引入形变因子前后性能指标雷达图。图 9 中，①～⑤分别表示 AUC、准确率、精准率、召回率和 F1 分数。由图 9 可知：在未引入形变动态因子时，SVM 模型综合性能最优，其次为 CNN，RF 模型相对较弱，SVM 与

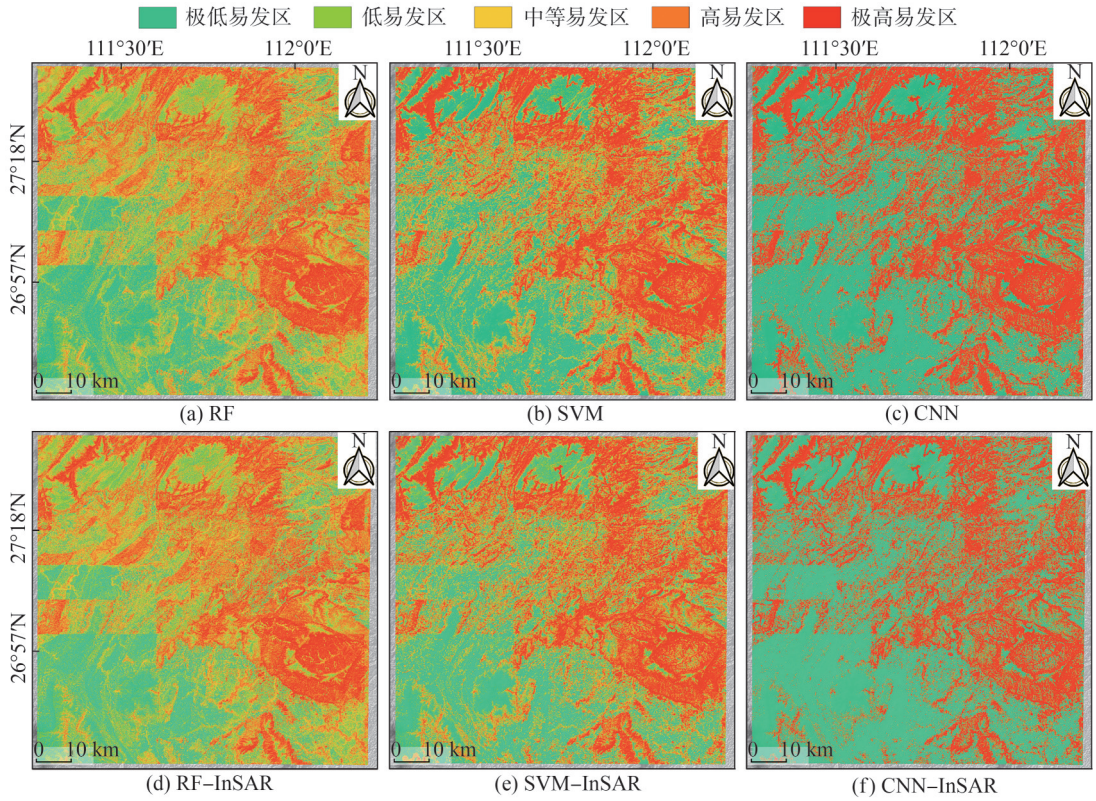


图 8　各模型滑坡易发性分区

Fig. 8　Landslide susceptibility maps of different models

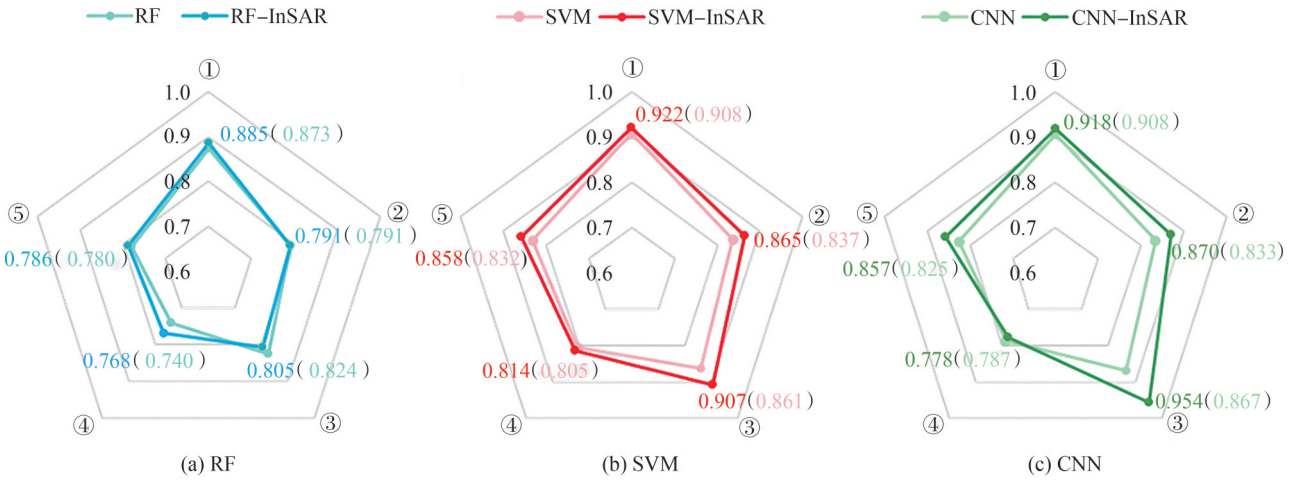


图9 各模型引入形变因子前后性能指标雷达图

Fig. 9 Radar chart of performance indexes of each model before and after incorporating deformation factors

CNN的AUC值相当，但均比RF模型高出约4%；在其余指标上，SVM的预测结果略优于CNN，表现出较好的综合性能；引入形变动态因子后，RF–InSAR除精准率外其余指标均有所提升；CNN–InSAR除召回率外各项性能指标均有所提升；而SVM–InSAR所有性能指标均上升；SVM–InSAR的AUC值分别比RF–InSAR和CNN–InSAR高出约4.2%和0.4%，表明SVM和CNN模型性能接近，但SVM–InSAR表现最优。综上，InSAR因子的引入能够有效提升模型预测能力，其中SVM模型的改进最为明显。

3.4 典型滑坡形变分析

结合第3.2和3.3节可知，SVM–InSAR模型在滑坡易发性评价中表现最优。基于此，进一步基于该模型提取犬木塘灌区各灌片的滑坡易发性分布情况，其内像元统计、ROC曲线、滑坡易发性评价结果分别见表3和图10、11。按高与极高易发性面积占比排序，邵峰直灌片、流光岭片和三都宝田片分别为78.50%、58.87%和58.56%，均超过各灌片总面积的一半，表明这些区域的环境特性显著增加了滑坡发生的可能性；同时，虽然三都宝田片、南充力群片和黄家坝三合片的高和极高易发区的面积占比小于40%，但其总面积分别达到119.77 km^2、125.82 km^2和99.20 km^2，说明这些区域仍存在较大潜在滑坡隐患；相对而言，上福冲、江口和唐福冲等13个灌片区域内滑坡高与极高易发性面积较低，主要零星分布于灌区的北部或西部。针对上述区域，建议持续开展In-

表3 灌片不同易发区内像元统计

Tab. 3 Statistical of pixels in different areas of irrigation area

灌片名称	易发性区间内像元数量					高易发性与极高易发性	
	极低	低	中等	高	极高	占比/%	面积/km^2
邵峰直灌片	3 809	7 609	12 004	21 163	64 369	78.50	76.97
流光岭片	18 075	20 223	24 045	31 442	57 799	58.87	80.31
三都宝田片	21 782	33 503	38 880	48 218	84 869	58.56	119.77
南充力群片	99 815	70 708	61 350	59 813	79 991	37.61	125.82
黄家坝三合片	81 935	59 552	53 956	54 331	55 901	36.06	99.20
上福冲片	23 751	20 618	17 157	15 063	14 675	32.58	26.76
江口片	47 031	20 649	15 523	16 150	23 371	32.20	35.56
唐福冲片	28 074	17 316	13 299	11 755	13 276	29.90	22.52
祁东直灌片	20 341	17 515	13 557	10 213	9 255	27.47	17.52
铁塘桥片	18 826	15 289	11 241	8 587	7 163	25.77	14.17
曹口堰片	50 680	26 360	19 759	16 358	15 877	24.98	29.01
里雅塘片	11 270	5 530	3 457	2 642	3 771	24.05	5.77
双清片	10 457	6 155	4 444	3 259	2 150	20.44	4.86
杨家台片	84 147	42 992	28 831	21 116	16 340	19.36	33.71
九公桥支渠片	25 457	14 935	9 696	6 310	3 453	16.31	8.78
黑冲峡口山片	78 633	31 745	19 674	14 060	9 859	15.53	21.52
茶园冲片	26 667	5 910	3 193	2 085	1 089	8.15	2.85
龙江桥片	149 743	40 185	21 349	11 847	5 318	7.51	15.44
大祥片	39 006	11 481	5 729	2 739	699	5.76	3.09

SAR 形变监测，以实现滑坡灾害的长期动态监控。

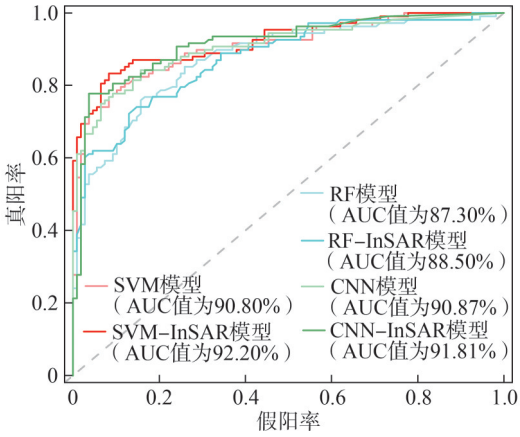


图 10　ROC 曲线

Fig. 10　Curves of ROC

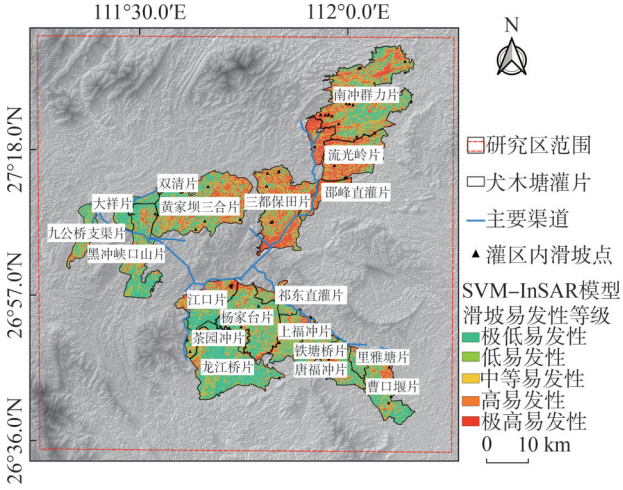


图 11　犬木塘灌片滑坡易发性评价结果

Fig. 11　Evaluation results of landslide susceptibility of Quanmutang irrigation area

4　结论与展望

4.1　结论

为实现山区水利工程滑坡隐患识别与概率预测，以犬木塘灌区工程为研究对象，基于 SBAS–InSAR 技术获取了研究区地表形变速率并识别了滑坡隐患。在此基础上，选取了高程、坡向、曲率、平面曲率、剖面曲率、坡度、地形湿度指数、距水系距离、距道路距离、距断层距离、土地利用、地层年代、植被指数和降雨量共 14 个因子构建滑坡易发性评价指标体系，并分别构建 RF、SVM 和 CNN 模型开展滑坡易发性评价，同时引入 InSAR 形变速率动态因子对模型进行优化，主要结论如下：

1）RF、SVM 和 CNN 这 3 类模型获得较为一致的滑坡易发性空间分布。极低与低易发区主要分布于研究区的西南部，高与极高易发区主要集中于西部和北部山区，与历史滑坡分布总体一致。不同易发区与近 5 a 平均降雨量分布高度吻合，表明降雨是影响滑坡易发性的重要因素，且该结论与特征重要性分析结果一致。

2）3 类模型都具有良好的预测性能，AUC 值均高于 0.85。其中，SVM 模型表现最优，其次为 CNN 模型，RF 模型相对较弱。引入 InSAR 形变动态因子后，各模型性能指标均有所提升，其中，SVM–InSAR 模型综合性能表现最佳，AUC 值分别较 RF–InSAR 和 CNN–InSAR 提升约 4.2% 和 0.4%，表明融合时序 InSAR 技术的滑坡易发性评价方法能够有效提升滑坡易发性评价精度。

3）犬木塘灌区工程不同灌片的易发区像元统计结果表明，邵峰直灌片、流光岭片和三都宝田片中高与极高易发区面积占比分别为 78.50%、58.87% 和 58.56%，均超过各灌片总面积的一半，表明上述区域滑坡发生风险较高，其余地区亦存在不同程度的滑坡风险，亟须持续监测与防范。

综上，本文将时序 InSAR 形变监测与滑坡易发性评价模型相结合，为山区水利工程滑坡风险识别与监测提供了新的技术路径，可为滑坡灾害预警、防控及工程规划建设提供参考。

4.2　展望

山区水利工程滑坡灾害的发生通常受地形地貌、地质结构、水文气候及工程活动等多因素综合影响。本文选取的评价因子存在一定局限性，未来研究可进一步结合水利工程建设对地质环境与水文条件的影响，优化滑坡易发性评价因子的筛选方法，以提高评价结果的工程适用性。

在因子标准化处理方面，本文采用信息量法对评价因子进行无量纲处理，虽能消除因子间量纲差异，但难以揭示不同因子对滑坡易发性的相对贡献。未来可结合权重思想，对评价因子的重要性进一步量化。

此外，本文采用自然断点法对因子及评价结果进行分级，虽具有操作简便等优点，但在复杂工程环境下仍需进一步优化。未来研究可结合无监督机器学习方法优化分级区间，以系统探讨分级方法对模型预测精度和适用性的影响。

综上，未来研究需进一步完善因子选择、权重分配和分级方法等，以不断提升山区水利工程滑坡风险识别与预警的科学性和可靠性。

参考文献：

[1] Liu Chuanzheng,Shen Weizhi,Huang Shuai.Some viewpoints on strategies in risk reduction of geological disasters in China[J].Journal of Catastrophology,2022,37(3):1–4.[刘传正，沈伟志，黄帅．中国地质灾害预防应对战略思考[J]．灾害学，2022,37(3):1–4.]

[2] Zhang Xingfu,Jiang Yuanjun,A Bierdi.Rainfall-induced landslide susceptibility prediction considering spatial hete-

rogeneity[J]. Advanced Engineering Sciences, 2025, 57(4): 12–28.[张幸福,姜元俊,阿比尔的.考虑空间异质性的降雨滑坡易发性预测研究[J].工程科学与技术,2025,57(4): 12–28.]

[3] Petley D.Global patterns of loss of life from landslides[J]. Geology,2012,40(10):927–930.

[4] Shang Min,Yuan Shuo,Wang Dianpeng,et al.The deformation characteristics and surge wave prediction of the Heishiban landslide in the Three Gorges Reservoir area[J].Journal of Hydraulic Engineering, 2024, 55(10): 1236–1247.[尚敏,袁朔,王殿鹏,等.三峡库区黑石板滑坡的变形特征和涌浪预测[J].水利学报,2024,55(10):1236–1247.]

[6] Liu Wei.Investigation,statistics and analysis of geological disasters in China[J].Mining Technology,2021,21(5):100–103.[刘伟.我国地质灾害调查统计与分析[J].采矿技术,2021,21(5):100–103.]

[7] Lan Yingying,Guo Changcheng,Zhu Yunfu.Review on the evaluation methods of geological hazard susceptibility[J]. Geology and Resources,2024,33(1):65–73.[兰盈盈,郭昶成,朱云福.地质灾害易发性评价方法综述[J].地质与资源,2024,33(1):65–73.]

[8] Duan Zhongman, Luo Weiqi, Chen Yana, et al. Analysis of landslide disaster susceptibility based on information quantity and machine learning: Take the central and western regions of Hunan Province as an example[J].Journal of Natural Science of Hunan Normal University, 2024, 47(5): 111–120.[段中满,罗伟奇,陈雅娜,等.基于信息量和机器学习的滑坡灾害易发性分析——以湖南省中西部地区为例[J].湖南师范大学自然科学学报,2024,47(5):111–120.]

[9] Zhang Wei, Chen Hong, Ji Chengliang, et al. Landslide susceptibility assessment in the Alpine and canyon areas on the basis of ascending and descending InSAR data[J]. Bulletin of Geological Science and Technology, 2025, 44(2): 94–103.[张伟,陈宏,纪成亮,等.基于升降轨InSAR数据的高山峡谷区滑坡易发性评价[J].地质科技通报,2025,44(2): 94–103.]

[10] Xu Yuanmao,Wu Zhen,Liu Jie.Early identification of potential landslide hazards and precipitation correlation analysis in Zhouqu County based on SBAS–InSAR technology[J]. Advanced Engineering Sciences,2023,55(6):257–271.[徐源懋,武震,刘杰.基于SBAS–InSAR技术的舟曲县潜在滑坡灾害早期识别及降水相关性分析[J].工程科学与技术,2023,55(6):257–271.]

[11] Yang Jiayi, Yang Chengsheng, Wei Yunjie, et al. Monitoring of Yunnan cheyiping landslide activities and analysis of influencing factors based on time series InSAR technology[J]. Journal of Geodesy and Geodynamics,2025,45(1):13–21.[杨佳艺,杨成生,魏云杰,等.基于时间序列InSAR技术的云南车邑坪滑坡活动监测及影响因素分析[J].大地测量与地球动力学,2025,45(1):13–21.]

[12] Wang Shenhe,Wang Shijie.Influence of water level fluctuation on landslide deformation in Baihetan reservoir area[J]. Progress in Geophysics,2025,40(1):94–105.[王深禾,王世杰.白鹤滩库区水位波动对滑坡形变的影响[J].地球物理学进展,2025,40(1):94–105.]

[13] Ferretti A,Prati C,Rocca F.Permanent scatterers in SAR interferometry[J].IEEE Transactions on Geoscience and Remote Sensing,2001,39(1):8–20.

[14] Berardino P,Fornaro G,Lanari R,et al.A new algorithm for surface deformation monitoring based on small baseline differential SAR interferograms[J]. IEEE Transactions on Geoscience and Remote Sensing,2002,40(11):2375–2383.

[15] Zhang Yongshuang, Liu Xiaoyi, Yao Xin. InSAR–based method for early recognition of ancient landslide reactivation in Dadu River, China[J]. Journal of Hydraulic Engineering,2020,51(5):545–555.[张永双,刘筱怡,姚鑫.基于InSAR技术的古滑坡复活早期识别方法研究——以大渡河流域为例[J].水利学报,2020,51(5):545–555.]

[16] Dong Yujuan, Zuo Xiaoqing, Li Yongfa, et al. DS–InSAR-based deformation monitoring and LandslideIdentification in reservoir area of a power station in southwest China[J]. Remote Sensing Information, 2024, 39(1): 104–111.[董玉娟,左小清,李勇发,等.基于DS–InSAR的西南某电站库区形变监测及滑坡体识别[J].遥感信息,2024,39(1): 104–111.]

[17] Wan Peng,Han Xianquan,Tan Yong,et al.TD–InSAR monitoring of land surface deformation along WaterDiversion Projects based on cloud computing[J].Journal of Changjiang River Scientific Research Institute, 2024, 41(10): 206–214.[万鹏,韩贤权,谭勇,等.基于云计算的引调水工程星载TD–InSAR地表形变监测[J].长江科学院院报,2024,41(10):206–214.]

[18] Wang Yian, Dong Jie, Zhang Lu, et al. Automatic detection and update of landslide inventory before and after impoundments at the Lianghekou reservoir using Sentinel–1 InSAR[J]. International Journal of Applied Earth Observation and Geoinformation,2023,118:103224.

[19] Bian Shiqiang, Chen Guan, Zeng Runqiang, et al. Post-failure evolution analysis of an irrigation-induced loess landslide using multiple remote sensing approaches integrated with time-lapse ERT imaging: Lessons from Heifangtai,China[J]. Landslides,2022,19(5):1179–1197.

[20] Zhu Yifei, Yao Xin, Yao Leihua, et al. Detection and characterization of active landslides with multisource SAR data and remote sensing in western Guizhou, China[J]. Natural Hazards,2022,111(1):973–994.

[21] Saaty T L,Vargas L G.Estimating technological coefficients by the analytic hierarchy process[J]. Socio－Economic Planning Sciences,1979,13(6):333–336.

[22] Su Jianhui, Li Yongcai, Dou Shun. Analysis of highway slope stability by fuzzy comprehensive evaluation[J].Subgrade Engineering,2015(5):38–42.[苏建辉,李永才,窦顺.基于模糊综合评判法分析某公路边坡稳定性[J].路基工程,2015(5):38–42.]

[23] Di Jingyue, Xu Hui, Xu Fengwen, et al. Benefit assessment of geological hazard meteorological services based on inverse algorithm and evaluation method of Delphi[J]. Meteorological Monthly,2019,45(5):705–712.[狄靖月,徐辉,许凤雯,等.基于逆推法和德尔菲法的地质灾害气象服务效益评估[J].气象,2019,45(5):705–712.]

[24] Wang Jiani,Wang Yunqi,Li Yaoming,et al.Landslide susceptibility assessment based on weighted information value model: A case study of Chongqing City[J]. Science of Soil and Water Conservation,2023,21(6):53–62.[王佳妮,王云琦,李耀明,等.基于信息量模型的滑坡灾害易发性评价——以重庆市为例[J].中国水土保持科学(中英文),2023,21(6):53–62.]

[25] Hu Xiuyu,Qin Shengwu,Dou Qiang,et al.Susceptibility analysis of debris flow based on GIS and random forest—A case study of a mountainous area in northern Taonan City, Jilin Province[J]. Bulletin of Soil and Water Conservation,2019,39(5):204–210.[扈秀宇,秦胜伍,窦强,等.基于GIS和随机森林模型的泥石流敏感性分析——以吉林省洮南市北部山区为例[J].水土保持通报,2019,39(5):204–210.]

[26] Huang Wubiao, Ding Mingtao, Li Zhenhong, et al. An efficient user-friendly integration tool for landslide susceptibility mapping based on support vector machines: SVM－LSM toolbox[J].Remote Sensing,2022,14(14):3408.

[27] Pan Wangsheng, Zhao Tianyin, Yu Xiulian, et al. Landslide susceptibility assessment in Huangling County based on probability ratio and support vector machine model[J]. Journal of Natural Disasters,2024,33(4):48–59.[潘网生,赵恬茵,蔚秀莲,等.基于PR–SVM模型的黄陵县滑坡易发性评价[J].自然灾害学报,2024,33(4):48–59.]

[28] Li Chenglin,Liu Yansong,Lai Sihan,et al.Landslide susceptibility analysis based on the coupling model of logistic regression and support vector machine[J].Journal of Natural Disasters,2024,33(2):75–86.[李成林,刘严松,赖思翰,等.基于逻辑回归和支持向量机耦合模型的滑坡易发性分析[J].自然灾害学报,2024,33(2):75–86.]

[29] Zhang Yuhan, Hu Jiang, Li Xing. Multi-source data-driven analysis of deformation and influencing factors for expansive soil canal slopes[J]. Advanced Engineering Sciences, 2026,58(3):270–282.[张妤涵,胡江,李星.多源数据驱动的膨胀土渠道边坡变形及影响因素分析方法[J].工程科学与技术,2026,58(3):270–282.]

[30] Zhang Ao,Zhao Xinwen,et al.Comparative study of different machine learning models in landslide susceptibility assessment: A case study of Conghua District, Guangzhou, China[J].China Geology,2024,7(1):104–115.

[31] Huang Xiaohu, Guo Fei, Deng Maolin, et al. Understanding the deformation mechanism and threshold reservoir level of the floating weight-reducing landslide in the Three Gorges Reservoir Area, China[J]. Landslides, 2020, 17(12): 2879–2894.

[32] Zhou Xiaoting, Huang Faming, Wu Weicheng, et al. Regional landslide susceptibility prediction based on negative sample selected by coupling information value method[J]. Advanced Engineering Sciences,2022,54(3):25–35.[周晓亭,黄发明,吴伟成,等.基于耦合信息量法选择负样本的区域滑坡易发性预测[J].工程科学与技术,2022,54(3):25–35.]

[33] Ding Jiawei, Wang Xiekang. Landslide and collapse susceptibility analysis in Wenchuan earthquake-damaged area based on ensemble learning methods[J].Advanced Engineering Sciences,2025,57(4):52–61.[丁嘉伟,王协康.基于集成学习方法的汶川震损区崩塌滑坡易发性评价[J].工程科学与技术,2025,57(4):52–61.]

[34] Su Zhiping, Yang Chengsheng, Wang Ziqian. Landslide susceptibility assessment in Nujiang canyon using negative sample optimization and machine learning models[J]. Journal of Geo-Information Science, 2025, 27(4): 979－993.[苏志萍,杨成生,王子倩.结合负样本优化与机器学习模型的怒江洲峡谷段滑坡易发性评价[J].地球信息科学学报,2025,27(4):979–993.]

[35] Wang Shouhua, Wang Ruisong, Sun Xiyan, et al. Landslide Susceptibility Evaluation Based on CF–CNN–LSTM Model [J].Journal of Natural Disasters,2024,33(5):84–95.[王守华,王睿菘,孙希延,等.基于CF–CNN–LSTM模型的滑坡易发性评价[J].自然灾害学报,2024,33(5):84–95.]

[36] Wubalem A, Meten M. Landslide susceptibility mapping using information value and logistic regression models in Goncha Siso Eneses area,northwestern Ethiopia[J].SN Applied Sciences,2020,2(5):807.

[37] Wu Liyang, Zeng Taorui, Liu Xiepan, et al. Landslide susceptibility assessment based on ensemble learning modeling[J]. Earth Science,2024,49(10):3841–3854.[邬礼扬,曾韬睿,刘谢攀,等.基于集成学习建模的滑坡易发性评价[J].地球科学,2024,49(10):3841–3854.]

[38] Huang Faming, Zhang Yinlang, Guo Zizheng, et al. Effects of different classification methods on regional landslide susceptibility zonation[J].Advanced Engineering Sciences,

2024,56(1):148–159.[黄发明,张鉴琅,郭子正,等.不同分级方法对区域滑坡易发性区划的影响[J].工程科学与技术,2024,56(1):148–159.]

[39] Liu Shandong, Li Jun, Jiang Xingyuan, et al. Optimization of landslide susceptibility assessment method coupling mathematical statistics and machine learning models[J]. Science Technology and Engineering, 2025, 25(5): 1827–1839.[刘山东,李军,江兴元,等.基于数学统计与机器学习模型耦合的滑坡易发性评价方法优化[J].科学技术与工程,2025,25(5):1827–1839.]

[40] Liu Shaoze, Cui Meijuan, Fu Xiaoyi, et al. Random forest evaluation of geological hazard susceptibility considering buffer range and negative sample optimization[J]. Science Technology and Engineering, 2025, 25(15): 6220–6229.[刘少泽,崔美娟,付晓祎,等.顾及缓冲区范围与负样本优化的随机森林地质灾害易发性评价[J].科学技术与工程,2025,25(15):6220–6229.]

Evaluation of Landslide Susceptibility for Irrigation Engineering Area with Temporal InSAR Technology

WANG Chenhao[1,2], *ZHOU Jun*[3], *DENG Bin*[1,2*], *HE Peiting*[1], *OUYANG Jun*[4], *YU Wenjie*[1,4], *JIANG Changbo*[1,2]

(1.School of Hydraulic and Ocean Engineering, Changsha University of Science & Technology, Changsha 410114, China;
2.Key Laboratory of Dongting Lake Aquatic Eco-environmental Control and Restoration of Hunan Province, Changsha 410114, China;
3.Hunan Provincial Water Resources Development and Investment Co., Ltd., Changsha 410007, China;
4.Hunan Water Resources and Hydropower Survey, Design, Planning and Research Co., Ltd., Changsha 410007, China)

Abstract:

Objective Mountainous hydraulic engineering projects are commonly constructed in regions characterized by complex geological structures, steep terrain, and strong hydro-meteorological influences. These conditions create a highly dynamic geomorphic environment in which landslides frequently occur and may pose severe threats to infrastructure safety, regional ecological stability, and sustainable socioeconomic development. Irrigation districts in mountainous areas are particularly vulnerable because the construction and operation of hydraulic facilities, such as canals, aqueducts, and slope excavations, often alter the original stress state of slopes and disturb the geological environment. Under the combined effects of rainfall infiltration, geological structures, and engineering disturbances, slope stability may gradually decrease, leading to landslide occurrence. Therefore, accurately identifying landslide-prone areas and quantitatively evaluating landslide susceptibility are essential for hazard prevention, infrastructure protection, and the long-term management of hydraulic engineering systems. Against this background, this study takes the Quanmutang Irrigation District in Hunan Province, China, as a representative mountainous hydraulic engineering area. The main objective is to develop a landslide susceptibility assessment framework that integrates time-series InSAR deformation information with machine learning models. Specifically, this research aims to 1) identify potential landslide hazards in the study area using SBAS–InSAR-derived deformation velocity; 2) construct a comprehensive landslide susceptibility evaluation system based on multisource environmental factors; 3) compare the predictive performance of multiple machine learning models; and 4) investigate the contribution of InSAR-derived deformation factors to improving the accuracy of landslide susceptibility assessment.

Methods To achieve the above objectives, a multisource data-driven landslide susceptibility assessment framework was established by integrating time-series InSAR analysis, information value modeling, and machine learning algorithms. First, surface deformation monitoring was conducted using the SBAS–InSAR technique. A total of 210 Sentinel–1A ascending SAR images covering the period from July 18, 2020, to August 8, 2023, were collected, along with precise orbit ephemerides (POD) data. The SAR data were processed using the ISCE software platform, including image co-registration, interferogram generation, filtering, and phase unwrapping. Small baseline interferometric pairs were constructed using temporal and spatial baseline thresholds of 90 days and 500 m, respectively, with an average coherence threshold of 0.3. After screening, 321 interferometric pairs were generated. Time-series analysis and error correction were then performed to obtain the surface deformation velocity field across the study area. Based on the deformation results, potential landslide hazard zones were identified. Second, a comprehensive landslide susceptibility evaluation factor system was constructed. Initially, 16 candidate factors were selected from four categories: topography and geomorphology, geological conditions, natural environment, and human activities. These factors included elevation, slope, aspect, curvature, plan curvature, profile curvature, terrain wetness index, distance to rivers, distance to roads, distance to faults, land use type, geological age, normalized difference vegetation index, rainfall, terrain relief, and surface roughness. To avoid multicollinearity among variables, Pearson correlation analysis was conducted. Highly correlated factors were removed to reduce redundancy among the input variables. As a result, 14 static evaluation factors were retained. To eliminate the influence of differences in the scales of the factors, the information value method was employed for normalization. The information value model is a statistical approach based on information theory that quantifies the contribution of each factor category to landslide occurrence by comparing the spatial distribution of landslides with environmental conditions. The calculated information values were then used as input features for the machine learning models. Third, landslide susceptibility modeling was performed using three widely used machine learn-

ing algorithms: random forest (RF), support vector machine (SVM), and convolutional neural network (CNN). Landslide samples were compiled from two sources: 318 historical landslides recorded in the study area and 42 potential landslide hazards identified through InSAR deformation analysis, resulting in a total of 360 positive samples. A buffer zone of 1 000 m was established around these landslides to reduce spatial autocorrelation, and an equal number of non-landslide points were randomly generated outside the buffer zones as negative samples. The dataset was then divided into training and testing sets at a ratio of 70% and 30%, respectively. Finally, two sets of models were constructed for comparison: models using only static environmental factors and models incorporating InSAR-derived deformation velocity as an additional dynamic factor. Model performance was evaluated using multiple metrics derived from the confusion matrix, including the area under the receiver operating characteristic curve (AUC), accuracy, precision, recall, and F1–score.

Results and Discussions The landslide susceptibility maps produced by the RF, SVM, and CNN models exhibit similar spatial patterns. In general, low- and very-low-susceptibility zones are mainly distributed in the southwestern part of the irrigation district, where terrain conditions are relatively gentle and rainfall intensity is lower. In contrast, high- and very-high-susceptibility zones are concentrated in the western and northern mountainous areas. These regions are characterized by steep slopes, complex geological structures, and higher rainfall levels, which may promote slope instability through increased infiltration, elevated pore water pressure, and reduced effective stress in rock and soil masses. The susceptibility distribution also shows strong consistency with the spatial distribution of historical landslides, indicating that the models effectively capture the key environmental controls of landslide occurrence. Statistical analysis further reveals that rainfall plays an important role in landslide development in the study area, which is consistent with the feature importance analysis obtained from the machine learning models. Comparative evaluation of model performance indicates that all three machine learning models demonstrate good predictive capability. The AUC values of all models exceed 0.85, suggesting reliable classification performance. Among the three models, the SVM model achieves the highest overall performance, followed by the CNN model, whereas the RF model shows relatively lower accuracy. After incorporating InSAR-derived deformation velocity as a dynamic factor, the predictive performance of the models improves to varying degrees. For the RF−InSAR and CNN−InSAR models, several evaluation metrics show moderate improvements. In contrast, the SVM−InSAR model demonstrates consistent enhancement across all evaluation metrics. Its AUC value increases by approximately 4.2% compared with RF–InSAR and by 0.4% compared with CNN–InSAR, indicating that the SVM model benefits most from the integration of dynamic deformation information. Furthermore, statistical analysis of susceptibility zones across different irrigation subregions reveals that several areas exhibit particularly high landslide susceptibility. For example, the Shaofeng Direct Irrigation Area, Liuguangling Area, and Sandu Baotian Area have high- and very-high-susceptibility zones covering 78.50%, 58.87%, and 58.56% of their respective areas, indicating a high degree of landslide susceptibility. Although some other irrigation zones show lower proportions of high-susceptibility areas, their absolute areas remain significant, suggesting the presence of potential landslide-prone areas that require continuous monitoring.

Conclusions This study proposes a landslide susceptibility assessment framework that integrates time-series InSAR deformation monitoring with machine learning models for mountainous hydraulic engineering regions. By incorporating dynamic deformation information into the susceptibility modeling process, the proposed approach improves the identification of potential landslide-prone areas. The results demonstrate that the integration of InSAR–derived deformation velocity improves the predictive performance of landslide susceptibility models, particularly for the SVM model. The approach not only captures the static environmental conditions associated with landslide occurrence but also incorporates dynamic deformation information indicative of slope instability. From an engineering perspective, the susceptibility maps generated in this study provide valuable information for identifying areas with high landslide susceptibility within the Quanmutang Irrigation District. These results can support infrastructure planning, slope stability monitoring, and disaster prevention strategies in mountainous hydraulic engineering projects. Overall, the methodology developed in this study provides a practical framework for integrating remote sensing-based deformation monitoring with data-driven susceptibility modeling. The findings highlight the potential value of incorporating dynamic surface deformation information into landslide susceptibility assessment and provide technical support for landslide risk management, disaster prevention, and sustainable development in mountainous irrigation districts and similar engineering environments.

Key words: landslide susceptibility evaluation; SBAS–InSAR; machine learning model; convolutional neural network; Quanmutang irrigation

（编辑　周　璇）

引用格式：Wang Chenhao, Zhou Jun, Deng Bin, et al. Evaluation of landslide susceptibility for irrigation engineering area with temporal InSAR technology[J]. Advanced Engineering Sciences, 2026, 58(6): 268–281. [王陈浩，周俊，邓斌，等. 融合时序 InSAR 技术的灌区滑坡易发性评价[J]. 工程科学与技术，2026，58(6)：268–281.]